Clay Minerals, (2016) **51**, 715–722

Dissolution of the chrysotile structure in nitric-acid solutions at different pH

TERUHISA HONGO*

Work Environment Research Group, National Institute of Occupational Safety and Health, Japan, 6-21-1 Nagao, Tama-Ku, Kawasaki 214-8585, Japan

(*Received 10 June 2015; revised 18 June 2016; Editor: George Christidis*)

ABSTRACT: The nitric-acid dissolution of chrysotile was investigated with the aim of revealing the effect of pH on its structure. Chrysotile becomes more soluble at lower pH, with the octahedral, brucite sheet more readily dissolved than the tetrahedral sheet. The dissolution of the brucite sheet increases the pH of the solvent, because of the release of OH^- groups along with the Mg^{2+} ions. At pH 2.00, the characteristic cylindrical fibre bundle structure of chrysotile is retained after dissolution, although the outside surface of each fibre becomes rough. Chrysotile remains fibrous upon dissolution at pH 1.08, but the fibres are no longer crystalline and their cylindrical structure collapses. The nitric-acid treatments result in an increase in both the specific surface area and the pore volume of chrysotile.

KEYWORDS: Chrysotile, dissolution, layer silicate, pH.

Chrysotile is a naturally occurring fibrous 1:1 hydrated magnesium layer silicate. It forms as a secondary mineral resulting from the alteration of magnesium silicates, especially olivine, pyroxene and amphibole. Chrysotile, the idealized chemical formula of which is $Mg_3Si_2O_5(OH)_4$, consists of octahedral sheets of magnesium hydroxide (brucite) bonded covalently to tetrahedral SiO_2 sheets, yielding a regular layered structure (Brindley & Brown, 1980). The lattice parameter of the octahedral sheet is greater than that of the corresponding tetrahedral sheet. This structural mismatch causes internal stress which is released by the curvature of the layers. This in turn leads to the formation of characteristic tubular fibres with, depending on the origin of the material, internal and external diameters of 2–10 and ~20–50 nm, respectively, and with tetrahedral sheets forming the inner lining (Dana *et al.,* 1977). Naturally occurring bundles of chrysotile consist of regular sets of closely packed parallel nanofibres (Liu *et al.,* 2007).

* E-mail: hongo@h.jniosh.go.jp
Doi:10.1180/claymin.2016.051.5.02

Chrysotile is incombustible, chemically stable, thermally insulating and has a high electrical resistance. Its fibres are strong and very flexible (Foresti *et al.,* 2003). Chrysotile is, therefore, one of the most important inorganic materials for industrial and technological applications, its most widespread uses being as a friction material for brakes, in filtering devices, and in high-temperature seals. However, because of its implication in a number of pulmonary health issues, chrysotile has largely been replaced by safer alternatives. Nonetheless, many countries still use, import and export chrysotile, because so-called "controlled use" is often exempted from the existing trade ban (LaDou *et al.,* 2010).

The solubility of chrysotile is of interest to a wide range of disciplines, from hygiene and mineralogy to engineering. Since Hargreaves & Taylor (1946) reported that the magnesium in chrysotile may be removed by acid treatment, extensive research has been conducted on the dissolution of chrysotile. Particularly interesting in the context of the above-mentioned health issues is the potential conversion of fibrous chrysotile into non-hazardous phases by acid dissolution. Sugama *et al.* (1998) reported that chrysotile fibres are destroyed by dissolution in an aqueous

© 2016 The Mineralogical Society
https://doi.org/10.1180/claymin.2016.051.5.02 Published online by Cambridge University Press

solution of fluorosulfonic acid. Mineralogical approaches are also possible which exploit the weathering effect of the oxalate acid excreted by lichens (Favero-Long *et al.,* 2005). The biodurability of chrysotile has also been investigated using dissolution experiments, to understand the effects that lead to health problems such as mesothelioma and lung cancer (Hume & Rimstidt, 1992; Oze & Solt, 2010). Studies on chrysotile dissolution are also relevant to environmental engineering projects, with dissolved magnesium potentially allowing CO_2 fixation in the form of magnesium carbonate (Dlugogorski & Balucan, 2014).

A clear understanding of the structural and morphological alterations that occur upon dissolution is crucial to evaluate accurately the biodurability of chrysotile and its conversion to non-hazardous materials. Hume & Rimstidt (1992) conducted the experiment for dissolution of chrysotile at pH 2–6, and estimated the dissolution time using the experimental data from the silica release rate. Valentim *et al.* (2008) and Rozalen & Huertas (2013) investigated the dissolution using various acidic solutions. However, the above-mentioned studies were not focused on the dissolution effect on the structure and morphology; detailed study of the effects of dissolution on the tubular structure and structural changes to the dissolution rates of magnesium and silicon have not been reported. Furthermore, the dissolved residue has not been examined thoroughly microscopically. In particular, the dissolution effect on the fibre bundle has not been investigated and has not become apparent. In the present study, experimental dissolution of chrysotile at various pH values with nitric-acid solutions was performed. The effect of pH on the structure of chrysotile and dissolution rates of magnesium and silicon from the chrysotile sample was investigated. Moreover, the morphology and structure of the dissolved residue were studied by electron microscopy.

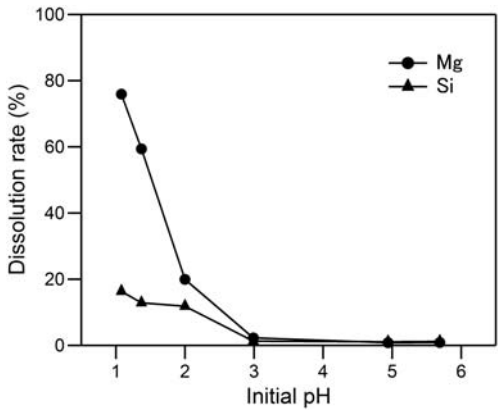


FIG. 1. Extent of dissolution of Mg and Si from raw chrysotile as a function of the initial pH.

EXPERIMENTAL

Dissolution of chrysotile

All experiments were carried out on chrysotile collected from the Coalinga mine in New Idria (California, USA). The chemical composition was (mass%) SiO_2 39.36, MgO 41.16, Fe_2O_3 3.26, CaO 0.42, Al_2O_3 0.41, Cr_2O_3 0.30 with an ignition loss of 14.50 mass%, and a Mg/Si atomic ratio of 1.56.

Dissolution experiments were carried out in batch reactors at a solid/solution ratio of 2.0 mg/L. The chrysotile sample was placed directly in polypropylene bottles containing 100 mL of either a nitric acid solution at pH 1.08–4.94 or ion-exchanged water at pH 5.69. The reaction bottles were immersed in a shaking water bath kept at 37°C for 10 days. The residual solids were centrifuged at 3000 rpm, washed three times with ion-exchanged water, and dried at 80°C for 24 h. The supernatant was filtered through a 0.20 μm sieve.

Analysis and characterization

The initial pH of the nitric-acid solutions and ion-exchanged water, and final pH of the filtrates were measured at room temperature with an Orion Star A121 portable pH-meter (Thermo Scientific). The concentrations of dissolved magnesium and silicon in the filtrates were determined using inductivity coupled plasma optical emission spectrometry (ICP-OES, PerkinElmer, Optima 7300 DV). X-ray diffraction (XRD) patterns were obtained with a Rigaku RINT 2000 diffractometer using Cu-*K*α radiation. Thermogravimetric and differential thermal analysis (TG-DTA) was conducted in air using a Rigaku Thermo plus EVO device. Room-temperature Fourier transform infrared (FTIR) spectra were recorded on a JASCO FT/IR 4100 spectrometer using KBr pellets. Field emission scanning electron microscopy (FE-SEM) images were obtained with an Hitachi S-4700 microscope, while transmission electron microscopy (TEM) observations were carried out on a JEOL JEM-2100 instrument operating at 200 kV. N_2 adsorption-desorption isotherms were measured at 77 K using a BELSORP-max instrument (MicrotracBEL, Japan). The specific surface areas were calculated using the

https://doi.org/10.1180/claymin.2016.051.5.02 Published online by Cambridge University Press

multi-point Brunauer-Emmett-Teller (BET) method and the pore sizes were calculated using the Barrett-Joyner-Halenda (BJH) approach.

RESULTS AND DISCUSSION

The extent of dissolution of Mg and Si from raw chrysotile as a function of the initial pH of the solution is shown in Fig. 1. The extent was calculated on the assumption that the chemical composition of the raw chrysotile was ideal (*i.e.* $Mg_3Si_2O_5(OH)_4$), without impurities. The amount of dissolution was clearly sensitive to the initial pH, with the dissolution of Mg and Si both increasing at lower pH values. The effect of the pH was greater on Mg than on Si. Indeed, whereas the dissolution rate for both elements is ~1% at pH 5, at pH 1.08, the dissolution rate of Mg was approximately five times greater (75.9%) than that of Si (16.3%).

The pH values measured at the beginning and end of the dissolution experiments are listed in Table 1. The pH increases after dissolution for all samples. The fact that the Mg dissolution rate is high suggests that the increase in pH is due to the dissolution of the brucite sheets, with an associated release of OH^- and Mg^{2+} ions. It has been reported that chrysotile releases Mg^{2+} and OH^- ions in aqueous media up to a pH of 10.33, a similar value to that measured in the present study for a suspension of $MgOH_2$ (10.37) (Pundsack, 1955).

The XRD patterns obtained for raw chrysotile and for samples treated with nitric acid or ion-exchanged water are shown in Fig. 2. Two intense reflections were observed for raw chrysotile, at 12.14°2θ and 24.42°2θ, which are indexed to the (002) and (004) planes (d = 7.29 and 3.64 Å, respectively) in agreement with ICDD file No. 25-0645. Minor brucite and calcite impurities were also present (Fig. 2). Similar patterns were obtained for the samples treated at pH 4.94 with nitric acid and pH 5.69 with ion-exchange water. The chrysotile diffraction maxima decreased in intensity at pH 2.99, while those assigned to brucite and calcite disappeared at pH 2.00 and 4.94, respectively. The XRD pattern from the sample treated at pH 1.08 showed a broad hump at 15–30°2θ, attributed to amorphous silica, along with weak chrysotile peaks.

The TG-DTA curves recorded for raw chrysotile and for samples treated in nitric acid solutions at pH 2.00 and 1.08 are shown in Fig. 3. A moderate mass-loss event is observed at low temperature in the data recorded for raw chrysotile, with ~3.2 wt.% lost between 40 and 500°C. The endothermic peak at ~70°C with mass loss is attributed to the desorption of adsorbed water. The endothermic peaks at 389 and 566°C with mass loss may be related to the decomposition of brucite and calcite impurities, respectively (Cattaneo *et al.,* 2003; Viti, 2010). The major endothermic peak at 629°C, with mass loss between 580 and 750°C, reflects the dehydroxylation

TABLE 1. Solution pH values before and after the dissolution experiments.

Initial pH	Final pH
1.08	1.31
1.37	1.74
2.00	5.31
2.99	7.49
4.94	9.62
5.69	9.69

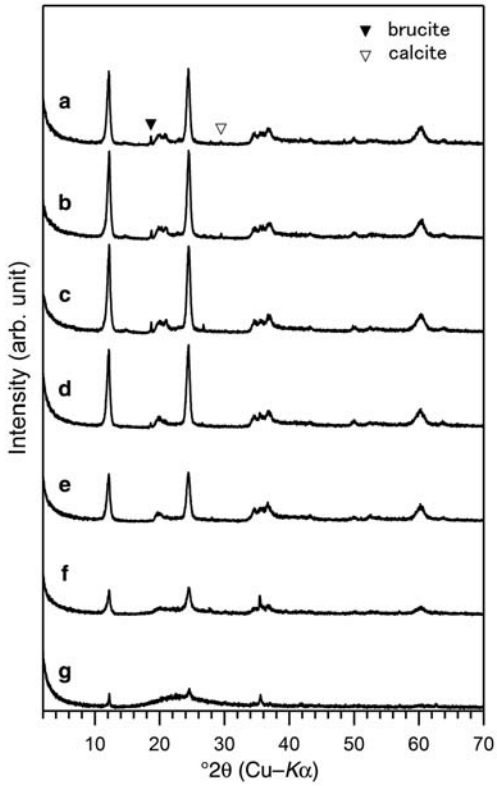


FIG. 2. XRD patterns obtained for chrysotile: (a) raw and (b–g) treated in (b) ion-exchanged water at pH 5.69 and (c–g) HNO_3 solutions at pH (c) 4.94, (d) 2.99, (e) 2.00, (f) 1.37 and (g) 1.08.

https://doi.org/10.1180/claymin.2016.051.5.02 Published online by Cambridge University Press

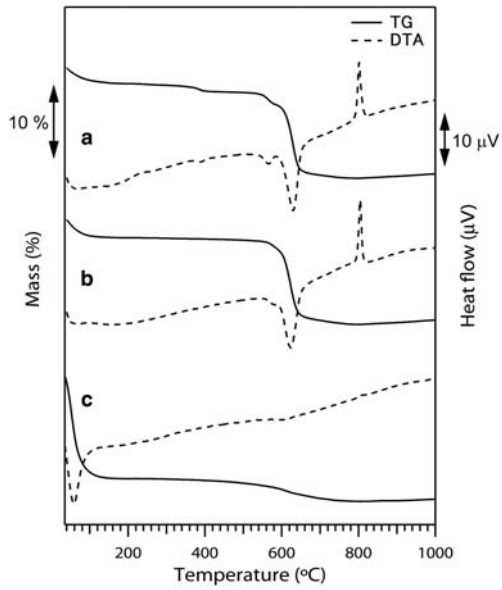


FIG. 3. TG-DTA curves recorded for chrysotile: (a) raw and (b, c) treated in HNO_3 solutions at pH (b) 2.00 and (c) 1.08.

chrysotile which leads to the complete breakdown of the mineral structure and the formation of an amorphous material, metachrysotile (Kusiorowski *et al.,* 2012). The exothermic peak at 802°C, without mass loss, corresponds to the recrystallization of the dehydroxylated phase and the formation of forsterite Mg_2SiO_4 (Viti, 2010). The mass remains constant above 800°C with a total mass loss of 14.5%, a value similar to that expected from the theoretical structural water content of chrysotile. In agreement with the XRD results, the endothermic peaks with mass loss attributed to the decomposition of brucite and calcite are not observed in the TG-DTA data for the sample treated at pH 2.00. The endothermic and exothermic peaks, at 614°C and 808°C, respectively, are weak for the sample treated at pH 1.08 due to the small amount of chrysotile, which remains undissolved. Instead, the TG curve obtained for this sample revealed two distinct mass-loss events characteristic of amorphous silica. The first step (at 40–200°C) is abrupt and is attributed to the removal of physisorbed water. The second, more gradual step (at 400–800°C) corresponds mainly to the release of chemisorbed water hydrogen-bonded to Si-OH groups (Vansant *et al*., 1995), with a smaller contribution from the decomposition of the residual chrysotile.

The effects of pH on the short-range order in chrysotile are highlighted in the FTIR spectra recorded for raw chrysotile and for samples treated in nitric-acid solutions at pH 2.00 or 1.08 (Fig. 4). The assignments of the different FTIR bands are based on those reported in previous studies (Van Der Marel & Beutelspacher, 1976; Anbalagan *et al.,* 2010). For raw chrysotile, stretching bands attributed to external and inner Mg-OH groups are observed at 3690 and 3642 cm^{-1}, respectively (Fig. 4a). The bands at 1084, 1020 and 957 cm^{-1} are attributed to Si-O-Si vibrations in the tetrahedral sheet, while the band at 607 cm^{-1} arises from inner Mg-OH vibrations and the peak at 434 cm^{-1} is due to Mg-OH translation or Si-O bending. The bands are somewhat broader for the sample treated at pH 2.00 (Fig. 4b). In the spectrum of the sample treated at pH 1.08 (Fig. 4c), the bands at 3443 and 1632 cm^{-1}, assigned to adsorbed water, are more intense than those recorded for raw chrysotile (Fig. 4a) indicating agreement with the TG-DTA results which suggested that the treated sample has a greater adsorbed water content. The shoulder at 3682 cm^{-1} is attributed to the stretching mode of inner Mg-OH groups in the undissolved chrysotile. The weakness of this band indicates that the brucite

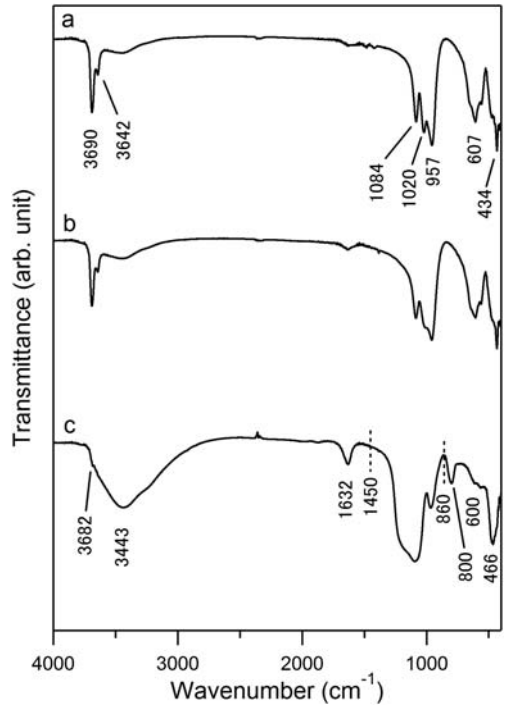


FIG. 4. FTIR spectra obtained for chrysotile: (a) raw and (b, c) treated in HNO_3 solutions at pH (b) 2.00 and (c) 1.08.

https://doi.org/10.1180/claymin.2016.051.5.02 Published online by Cambridge University Press

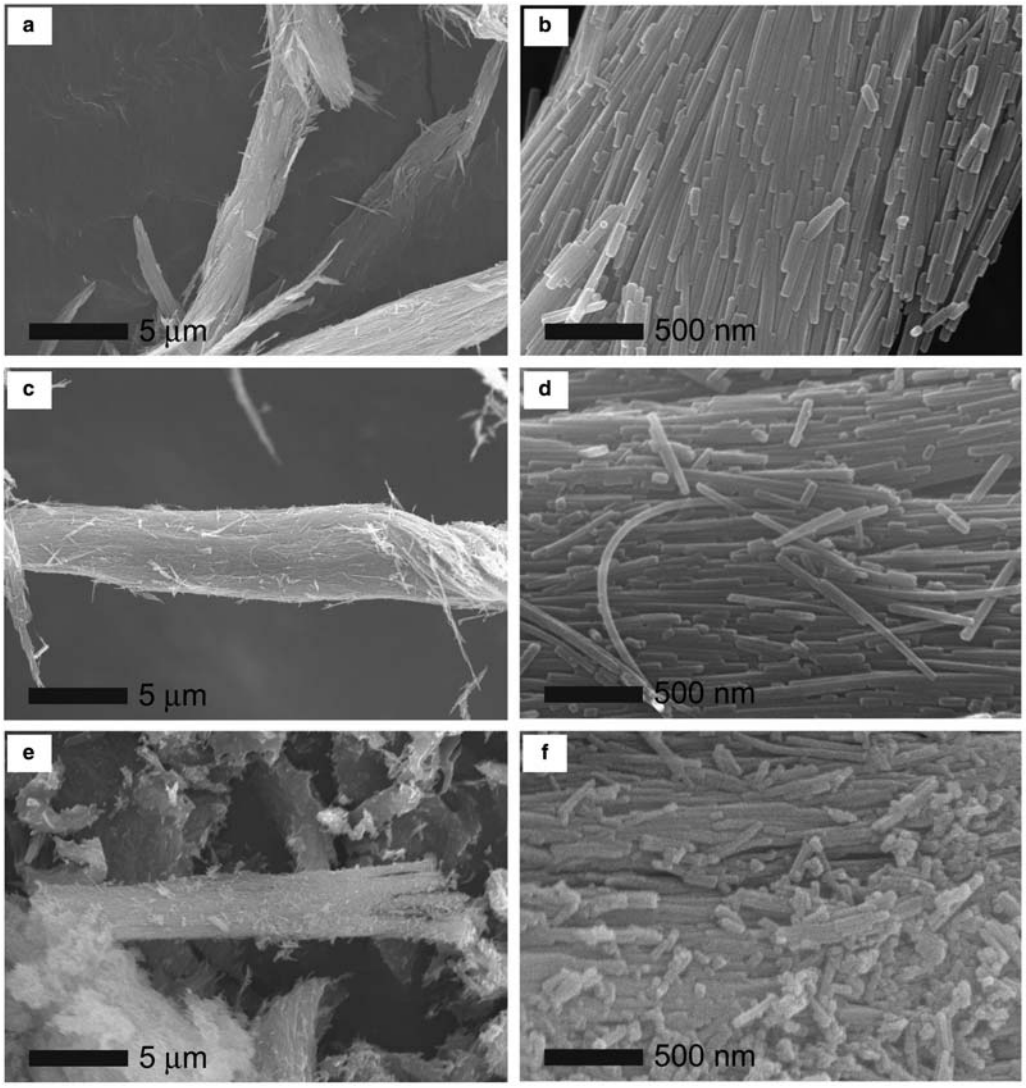


FIG. 5. (a, c, e) Standard and (b, d, f) high-magnification, field-emission SEM images of chrysotile: (a, b) raw and (b–f) treated in HNO_3 solutions at pH (c, d) 2.00 and (e, f) 1.08.

sheet in chrysotile has been destroyed (Mendelovici *et al.,* 2001). The acid-induced degradation of the octahedral sheet is greater for greater acid concentrations. The bands assigned to Si-O-Si vibrations between 860 and 1450 cm^{-1} broaden, with broad bands being characteristic of free SiO_2. This phenomenon has also been observed in other clay minerals subjected to acid attack, such as kaolinite and saponite (Kooli & Jones, 1997; Belver *et al.,* 2002). The additional band that appears at 800 cm^{-1} in Fig. 4c is due to the formation of free amorphous SiO_2. The band at 600 cm^{-1}, assigned to the vibration of inner Mg-OH groups, is much weaker than in Fig. 4a,b. Finally, the band at 466 cm^{-1} is assigned to Si-O-Si bending.

Under SEM the raw chrysotile displays heterogeneous bundles of chrysotile fibres (Fig. 5a). At greater magnification the alignment of the fibres becomes apparent (Fig. 5b). The fibres in each bundle are several tens of nanometers in diameter and vary in length from ~100 nm to well over 1 µm. No significant difference in morphology between the original sample and that treated at pH 2.00 was observed (Fig. 5a–d),

https://doi.org/10.1180/claymin.2016.051.5.02 Published online by Cambridge University Press

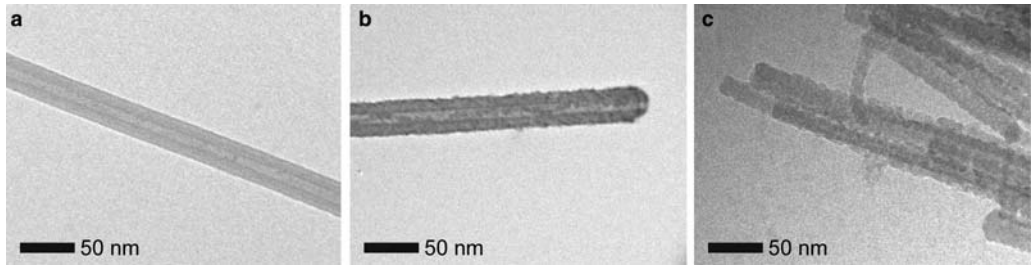


FIG. 6. TEM images of chrysotile: (a) raw and (b, c) treated in HNO_3 solutions at pH (b) 2.00 and (c) 1.08.

and a fibre bundle is also observed for the sample treated at pH 1.08 (Fig. 5e). Figure 5f shows, however, that for this sample the surface fibres are shorter (~10–100 nm) than those below. This indicates that dissolution proceeds from the surface towards the interior of the bundles, with the acid shortening and peeling the fibres on the surface and gradually thinning the bundle. This is consistent with a shrinking fibre model for chrysotile dissolution (Hume & Rimstidt, 1992).

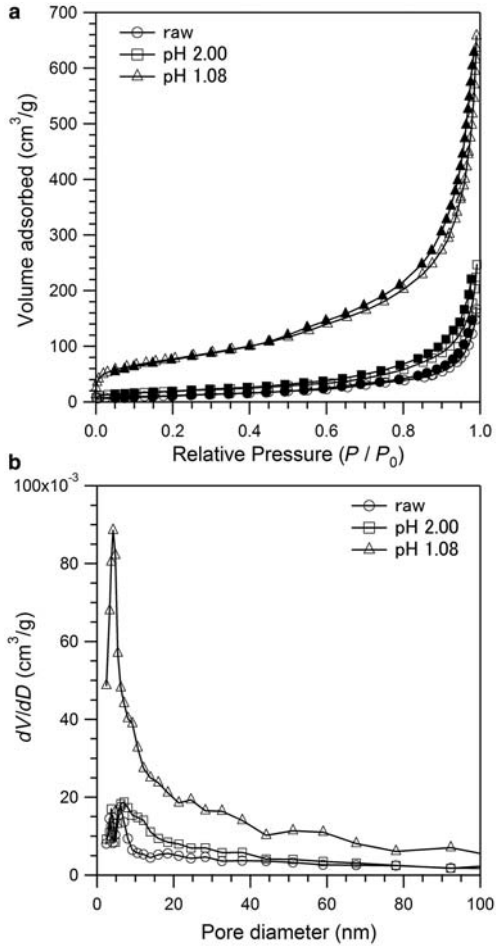


FIG. 7. (a) N_2 adsorption-desorption isotherms and (b) pore-size distribution curves of raw chrysotile and of samples treated in HNO_3 solutions at pH 2.00 or 1.08.

The TEM images obtained for raw chrysotile and for samples treated in nitric-acid solutions at pH 2.00 or 1.08 are shown in Fig. 6a–c. In raw chrysotile, the nanotubes have inner and outer diameters of 6–10 and 24–38 nm, respectively (Fig. 6a). The nanotubes in the sample treated at pH 2.00 have a similar cylindrical structure but their outer surface is rough (Fig. 6b). This suggests that acid attacks the outermost brucite sheet first. Fibres are also observed in the TEM image of the sample treated at pH 1.08 (Fig. 6c); however, their cylindrical structure has been destroyed, with separate inner and outer diameters being no longer apparent. The fibres are 14–30 nm in diameter, *i.e.* they are narrower than the untreated chrysotile nanotubes.

The nitrogen adsorption-desorption isotherms and BJH pore-size distribution plots of raw chrysotile and of samples treated in nitric acid solutions at pH 2.00 and 1.08 are shown in Fig. 7a,b. All of the samples presented small hysteresis loops at the range of $0.4 < P/P_0 < 1.0$, indicating the presence of mesopores. The sample treated at pH 1.08 showed increased adsorption in micropores at $P/P_0 < 0.1$. The specific surface areas of raw chrysotile and of samples treated at pH 2.00 and 1.08 were 42, 68 and 273 m^2/g, respectively, suggesting that the HNO_3 treatments increased the specific surface area compared to the raw chrysotile. In particular, the specific surface area of the sample treated at pH 1.08 was more than six times greater than that of the raw chrysotile. The pore-size distribution of raw chrysotile exhibits two maxima at 3.3 and 6.2 nm. The pore maximum at 3.3 nm is ascribed to the interparticle space between the fibres, and that at 6.2 nm is attributed to the inner diameter of the tubes. The same type of pore-size distribution exists in the sample

https://doi.org/10.1180/claymin.2016.051.5.02 Published online by Cambridge University Press

treated at pH 2.00, but the pore maxima are shifted slightly towards larger dimensions, i.e. 3.7 and 7.1 nm. The sample treated at pH 1.08 results in a significant increase in pore volume associated with the appearance of a large maximum at 4.2 nm. In agglomerates composed of SiO_2 nanoparticles in fibres, the mesopores are considered to consist of voids.

CONCLUSIONS

Chrysotile was dissolved at pH 5.69–1.08. Chrysotile becomes more soluble at lower pH values, especially below pH 2.99, whereby Mg is dissolved more readily than Si. At pH 1.08, the extent of dissolution of Mg is approximately five times greater than that of Si. The release of OH^- groups and Mg^{2+} ions from the brucite sheet increased the pH of the solvent after dissolution. Following dissolution at pH 2.00, the outer surface of the initially smooth chrysotile fibres became rough, but their cylindrical structure and the characteristic fibre bundles were retained. At pH 1.08, 75.8% of the magnesium was dissolved and TG-DTA, XRD and FTIR data revealed the formation of amorphous SiO_2. The fibrous nature of chrysotile was retained, nonetheless, in spite of the loss of crystal order and the collapse of the cylindrical structures. Further, as the pH of the nitric acid solution decreased, both the specific surface area and the pore volume increased.

ACKNOWLEDGEMENT

The author acknowledges gratefully Yasushi Shinohara of the National Institute of Occupational Safety and Health, Japan, for helpful advice during the experiments. The author also thanks Hironobu Abiko of the National Institute of Occupational Safety and Health, Japan for the measurement of N_2 adsorption-desorption isotherms. Editage (www.editage.jp) is acknowledged for assistance with the English language editing.

REFERENCES

Anbalagan G., Sivakumar G., Prabakaran S. & Gunasekaran S. (2010) Spectroscopic characterization of natural chrysotile. *Vibrational Spectroscopy*, **52**, 122–127.

Belver C., Bañares Muñoz A.B. & Vicente M.A. (2002) Chemical activation of a kaolinite under acid and alkaline conditions. *Chemistry of Materials*, **14**, 2033–2043.

Brindley G.W. & Brown G. (1980) *Crystal Structure of Clay Minerals and their X-ray Identification.* Monograph 5, Mineralogical Society, London.

Cattaneo A., Gualtieri A.F. & Artioli G. (2003) Kinetic study of the dehydroxylation of chrysotile asbestos with temperature by in situ XRPD. *Physics and Chemistry of Minerals*, **30**, 177–183.

Dana J.D., Hurlbut C.S. & Klein D. (1977) *Manual of Mineralogy.* John Wiley & Sons, New York.

Dlugogorski B.Z. & Balucan R.D. (2014) Dehydroxylation of serpentine minerals: Implications for mineral carbonation. *Renewable & Sustainable Energy Reviews*, **31**, 353–367.

Foresti E., Gazzano M., Gualtieri A.F., Lesci I.G., Lunelli B., Pecchini G., Renna E. & Roveri N. (2003) Determination of low levels of free fibres of chrysotile in contaminated solids by X-ray diffraction and FT-IR spectroscopy. *Analytical and Bioanalytical Chemistry*, **376**, 653–658.

Hargreaves A. & Taylor W.H. (1946) An X-ray examination of decomposition products of chrysotile (asbestos) and serpentine. *Mineralogical Magazine*, **27**, 204–216.

Hume L.A. & Rimstidt J.D. (1992) The biodurability of chrysotile asbestos. *American Mineralogist*, **77**, 1129–1128.

Kooli F. & Jones W. (1997) Characterization and catalytic properties of a saponite clay modified by acid activation. *Clay Minerals*, **32**, 633–643.

Kusiorowski R., Zaremba T., Piotrowski J. & Adamek J. (2012) Thermal decomposition of different types of asbestos. *Journal of Thermal Analysis and Calorimetry*, **109**, 693–704.

LaDou J., Castleman B., Frank A., Gochfeld M., Greenberg M., Huff J., Joshi T.K., Landrigan P.J., Lemen R., Myers J., Soffritti M., Soskolne C.L., Takahashi K., Teitelbaum D., Terracini B. & Watterson A. (2010) The case for a global ban on asbestos. *Environmental Health Perspectives*, **118**, 897–901.

Liu K., Feng Q., Yang Y., Zhang G., Ou L. & Lu Y. (2007) Preparation and characterization of amorphous silica nanowires from natural chrysotile. *Journal of Non-crystalline Solids*, **353**, 1534–1539.

Mendelovici E., Frost R.L. & Kloprogge J.T. (2001) Modification of chrysotile surface by organosilanes: An IR-photoacoustic spectroscopy study. *Journal Colloid and Interface Science*, **238**, 273–278.

Oze C. & Solt K. (2010) Biodurability of chrysotile and tremolite asbestos in simulated lung and gastric fluids. *American Mineralogist*, **95**, 825–831.

Pundsack F.L. (1955) The properties of asbestos. I. The colloidal and surface chemistry of chrysotile. *The Journal of Physical Chemistry*, **59**, 892–895.

Rozalen M. & Huertas F.J. (2013) Comparative effect of chrysotile leaching in nitric, sulfuric and oxalic acids at room temperature. *Chemical Geology*, **352**, 134–142.

Sugama T., Sabatini R. & Petrakis L. (1998) Decomposition of chrysotile asbestos by fluorosulfonic acid. *Industrial & Engineering Chemistry Research*, **37**, 79–88.

Valentim I.B., Martins M.H. & Joekes I. (2008) Influence of dipalmitoylphosphatidylcholine on the dissolution

https://doi.org/10.1180/claymin.2016.051.5.02 Published online by Cambridge University Press

of Brazilian chrysotile. *Colloids and Surfaces B*, **66**, 96–102.

Van Der Marel H.W. & Beutelspacher H. (1976) *Atlas of Infrared Spectroscopy of Clay Minerals and their Admixtures.* Elsevier Science, Amsterdam.

Vansant E.F., Van Der Voort P. & Vrancken K.C. (1995) *Characterization and Chemical Modification of the Silica Surface.* Elsevier Science, Amsterdam.

Viti C. (2010) Serpentine minerals discrimination by the thermal analysis. *American Mineralogist*, **95**, 631–638.

https://doi.org/10.1180/claymin.2016.051.5.02 Published online by Cambridge University Press